UPDATE E12-06-114: Measurements of the electron-helicity dependent cross-sections of deeply virtual Compton scattering in Hall A at 11 GeV

Spokespersons: A. Camsonne,[1] C. Hyde,[2] C. Muñoz Camacho,[3] and J. Roche[4]

[1] *Thomas Jefferson National Accelerator Facility, Newport News, Virginia 23606, USA*
[2] *Old Dominion University, Norfolk, Virginia 23529, USA*
[3] *Clermont Université, Université Blaise Pascal, CNRS/IN2P3, Laboratoire de Physique Corpusculaire, FR-63000 Clermont-Ferrand, France*
[4] *Ohio University, Athens, Ohio 45701, USA*

The Hall A Collaboration

This is an update on experiment E12-06-114, proposed to PAC30 (2006) and approved at that time. We review the scientific case for the proposal, emphasizing recent developments in the phenomenology of Generalized Parton Distributions (GPDs). In addition, we summarize the technical progress concerning the realization and upgrade of the necessary equipment. The experiment will measure the Q^2 dependence of the $\mathrm{H}(\vec{e},e'\gamma)p$ cross sections with a factor of 2 lever arm in Q^2 at each Bjorken-x point. The experiment does not require additional new equipment, beyond the 11 GeV upgrades to the beamline.

Contents

I. SCIENTIFIC CASE

Generalized Parton Distributions (GPDs) provide an unprecedented way to describe nucleon structure and thus help understand the transition between perturbative and non-perturbative QCD. Experimentally, GPDs can be accessed through hard exclusive processes, provided that the kinematics of the reaction are such that the main mechanism of the reaction is well described by its leading twist contribution. Physically, this corresponds to the limit where the virtual photon interacts with one single parton inside the nucleon.

Previous results by our collaboration [1] showed that Deeply Virtual Compton Scattering (DVCS) is particularly suited to study GPDs. Indeed, indications of early scaling (twist-2 dominance) were observed already at $Q^2 \sim 2$ GeV^2. However, the currently available 6 GeV beam provides a very limited lever arm in Q^2 in order to perform strong scaling tests of the DVCS amplitude.

The GPDs program is at the heart of the scientific motivation of the upgrade of Jefferson Lab to 12 GeV. In the new experiment we propose herein, we will perform much stronger tests of scaling (up to Q^2=9 GeV^2), and for central

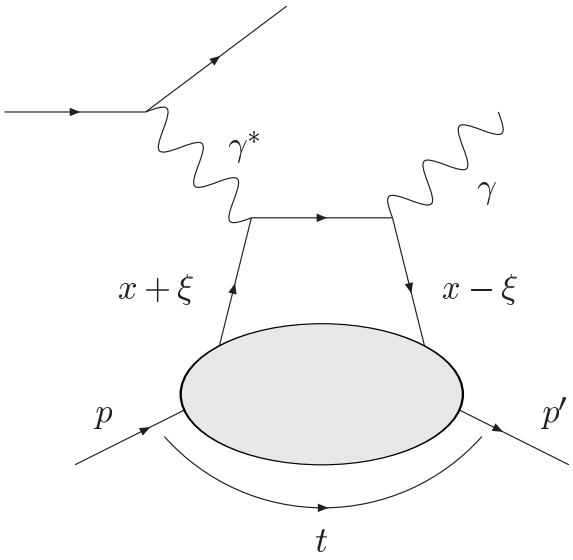

FIG. 1: Leading twist $\gamma^* p \to \gamma p$ amplitude in the DVCS limit. The initial and final quarks carry light-cone momentum fractions $x+\xi$ and $x-\xi$ of the light-cone momenta $(1 \pm \xi)(p+p')^+$. The crossed diagram is also included in the full DVCS amplitude. The invariant momentum transfer squared to the proton is $t = \Delta^2$. In the $t/Q^2 \to 0$ limit, the generalized Bjorken variable is defined by $\xi \to x_B/(2-x_B)$.

values of the Bjorken variable x_B from 0.36 to 0.60. By measuring separately, and as a function of Q^2, the unpolarized cross section and the helicity-dependent cross section, we will be able to provide independent tests of scaling for the real and the imaginary parts of the DVCS amplitude.

The specific scientific goals of this experiment are as follows:

- Measure the $\vec{e}p \to ep\gamma$ cross sections at fixed x_B over the full range in Q^2 accessible for $k \leq 11$ GeV. This will determine with what precision the handbag amplitude (Fig. 1) dominates (or not) over the higher twist amplitudes. At each x_B we have a factor of two range in Q^2, with all central Q^2 values ≥ 2 GeV^2.

- Extract all kinematically independent observables (unpolarized target) for each Q^2, x_B, t point. These observables are the angular harmonic superposition of Compton Form Factors (CFFs). As functions of the azimuth $\phi_{\gamma\gamma}$ of the real photon around the VCS virtual photon, the observable terms are $\cos(n\phi_{\gamma\gamma})$ for $n \in \{0,1,2\}$, and $\sin(n\phi_{\gamma\gamma})$ for $n \in \{1,2\}$, with additional calculable kinematic modulations from the electron propagators of the Bethe-Heitler (BH) amplitude in the interference terms. Each of these five observables isolates the $\Re$e or $\Im$m parts of a distinct combination of linear ($BH \cdot DVCS^\dagger$) and bilinear ($DVCS \cdot DVCS^\dagger$) terms.

- Measure the t-dependence of each angular harmonic term. The t-dependence of each CFF is Fourier-conjugate to the spatial distribution of the corresponding superposition of quark distributions in the nucleon, as a function of quark light-cone momentum-fraction. In a single experiment, we cannot access this Fourier transform directly, because we measure a superposition of terms. However, we still expect to observe changes in the t-dependence of our observables as a function of $\xi \approx x_B/(2-x_B)$. In particular, the *r.m.s.* impact parameter of a quark must diminish as the momentum fraction goes to unity. This is not a small effect, between $x_B = 0.36$ and $x_B = 0.6$, we expect a change in slope (as a function of t) of a factor two in individual GPDs.

- Measure the $\vec{e}p \to ep\pi^0$ cross section in the same kinematics as DVCS.

Ever since this proposal was submitted and accepted by PAC30 in 2006, the experimental collaboration has been active in the field. We have published 3 new papers [1–3], accomplished 2 new DVCS experiments (E07-007 and E08-025) and upgraded our equipment, which is now ready to run the 12 GeV experiment as soon as the beam is available. Notice also that several kinematics do not require the maximum beam energy. We indeed have kinematics at beam energies of 6.6, 8.8 and 11 GeV.

A. GPD Phenomenology

In the last few years since this proposal was accepted by PAC30 (2006), a number of theoretical and phenomenology papers have been published concerning the extraction of GPDs from data. This series of papers followed the publication of the DVCS cross-sections by the Hall A collaboration in 2006 [1] and the DVCS beam spin asymmetries (BSA) by the Hall B collaboration [4] in 2008. We review in the next section a few approaches that have been used in recent years.

At leading twist and leading order, the DVCS process is fully described by the four GPDs H, E, $\tilde{H}$ and $\tilde{E}$. They enter the cross section through Compton Form Factors (CFFs) which are defined at leading order as:

$$\mathcal{F} = \int_{-1}^{+1} dx\, F(x,\xi,t)\left(\frac{1}{\xi - x - i\epsilon} - \frac{1}{\xi + x - i\epsilon}\right) \qquad (F = H \text{ or } E) \tag{1}$$

$$= \mathcal{P}\int_{-1}^{+1} dx\, F(x,\xi,t)\left(\frac{1}{\xi - x} - \frac{1}{\xi + x}\right) + i\pi\Big(F(\xi,\xi,t) - F(-\xi,\xi,t)\Big) \tag{2}$$

The symbol $\mathcal{P}$ stands for the Cauchy principal value. A CFF is complex-valued and we note by Re CFF and Im CFF its real and imaginary parts. They are related by fixed-t dispersion relations [5–8], for example :

$$\mathrm{Re}\,\mathcal{H}(\xi,t) = 2\mathcal{P}\int_0^{+1} \frac{d\xi'}{\xi'} \frac{\mathrm{Im}\,\mathcal{H}(\xi',t)}{\frac{\xi^2}{\xi'^2} - 1} + \Delta(t) \tag{3}$$

where $\Delta(t)$ is a subtraction term related to the D-term in the GPDs [9]. A first attempt to use dispersion relations in the Hall A data [1] was made by M. Polyakov and M. Vanderhaeghen in 2008 [10]. However, the D-term is poorly known and most of the DVCS measurements were made in the region $\xi' \leq 0.5$. Using such dispersion relations thus relies on models and may introduce biases in the extraction of GPDs from DVCS data. For that reason the real and imaginary parts of CFFs are taken as independent in some fitting procedures.

B. Extraction of Generalized Parton Distributions from data

by H. Moutarde (CEA Saclay, Irfu/SPhN), common with E12-06-119

Extractions of GPDs is a much more demanding task than the extraction of Parton Distribution Functions (PDF) or Form Factors (FF) due to the complex functional structures of GPDs. Moreover, we need to extract four functions H, E, $\widetilde{H}$ and $\widetilde{E}$ of three variables (x,ξ,t) for each quark flavor (u, d and s). The Q^2-dependence is governed by the QCD evolution equations. Building a flexible yet robust GPD parametrization is very involved and the problem is still open today, but several groups have made attempts to fit GPDs (or CFFs) to data during the last few years. We will describe the different fitting methods in the following sections.

1. *Local fits of CFFs*

The first approach, pioneered in [11] and used in [12–15] assumes the independence of the real and imaginary parts of CFFs. The main assumptions are the validity of the twist-2 leading order analysis of existing DVCS measurements and a negligible contribution of $\mathrm{Im}\,\tilde{\mathcal{E}}$. Each kinematic bin (x_B, t, Q^2) is taken independently of the others, and the seven values $\mathrm{Re}\,\mathcal{H}$, $\mathrm{Im}\,\mathcal{H}$, $\mathrm{Re}\,\mathcal{E}$, $\mathrm{Im}\,\mathcal{E}$, $\mathrm{Re}\,\widetilde{\mathcal{H}}$, $\mathrm{Im}\,\widetilde{\mathcal{H}}$ and $\mathrm{Re}\,\widetilde{\mathcal{E}}$ are extracted simultaneously, so nothing prevents large fluctuations between two neighboring kinematic bins. Moreover this method gives no clue on the extrapolation of the extracted CFF outside the data region. In the following we will refer to these fits as *local fits*. The model-dependence is almost as low as possible but the problem is often under-constrained.

2. *Global fits of GPDs*

In the spirit of the work done on PDFs and FFs, *global fits* require a physically motivated parametrization of GPDs and deal with all observables on all kinematic bins at once. The main advantage is obvious : the ability to extrapolate outside of the data region, and therefore evaluate for instance Ji's sum rule ($t \to 0$) or more generally, study the 3D partonic structure of the nucleon ($\xi \to 0$). The free coefficients entering the expressions for GPDs are determined

either from PDFs and FFs or from DVCS data. Two such studies have been reported recently for DVCS [16, 17]. Note that fixed-t dispersion relations are used as a key ingredient in [16].

3. Hybrid fits of GPDs

The *hybrid* fitting procedure used in [12] is a combination of the previous two methods and has been applied with the main assumption of H-dominance and twist-2 accuracy. It involves a parametrization which fulfills the polynomiality condition of GPDs and includes Q^2 evolution at leading order in α_S. Since this function is otherwise arbitrary, its specific form is *a posteriori* validated by the quality of the fit. It makes it hazardous to extrapolate the extracted GPD outside the fitting domain as unphysical oscillations may occur. The model dependence is tested by a systematic comparison to local fits and an estimate of the systematic error induced by the H-dominance hypothesis. The good agreement of the local fits with respect to the global fits is a strong consistency check of this approach.

4. Neural network fits of GPDs

Neural network fits had been successfully performed for PDFs but their use for GPD extraction is quite recent. First results are described in [18] within the H-dominance assumption. Although it is too early to judge the advantages and shortcomings of this approach, it is worth noting that it is a new development in the field of GPD extraction.

In conclusion, the first extractions of GPDs or CFFs from early JLab and HERMES DVCS data are encouraging and a lot of progress has been made by the different groups involved. The abundance of 11 GeV data will allow for more flexible functional forms to be fitted, which will help to relax the drastic hypothesis made so far such as H-dominance, twist-2 dominance and leading order analysis. There is no doubt that in the coming years, several groups will refine their fitting machinery and will get ready to analyze a large quantity of data from the Jefferson Lab upgrade.

C. Neutral pion electroproduction

Together with DVCS data, a sample of π^0 events produced in the same deeply virtual kinematics as DVCS will be collected during this experiment. From our previous data, the collaboration has published π^0 electroproduction cross sections at 2 values of $Q^2 \sim 2$ GeV^2 [3]. While these results show that π^0 electroproduction is not well described by GPDs at these values of Q^2, the interpretation of the results have already stimulated several publication by theorists [19–22] suggesting alternate reaction mechanisms.

With the higher values of Q^2 accessible at JLab–12GeV, π^0 electroproduction cross section will remain very interesting results coming out of this DVCS experiment.

II. TECHNICAL PROGRESS: EXPERIMENTS E07-007 & E08-025

Since the current proposal was submitted to PAC30 in 2006, two new related experiments, E07-007 (PAC31) and E08-025 (PAC33) have been proposed and accepted. These two experiments ran concurrently during Fall 2010. We review in this section the performance of the equipment, as it is the same equipment we plan to use for E06-12-114.

A. Electromagnetic calorimeter

The DVCS calorimeter was upgraded for experiments E07-007/E08-025 (Fig. 2) and for E06-12-114. 76 new PbF_2 blocks were added to the previous 132, increasing the array from 11×12 to 13×16 blocks. This increases the acceptance for DVCS and π^0 events, taking advantage of the extra room available by the suppression of the recoil detector. Each additional channel was equipped with the same Hamamatsu PMTs.

Our new DVCS calorimeter was more radiation-hard than the previous one due to the selection of crystals. We had about 30 spare PbF_2 blocks. Before assembling the new calorimeter, each block was individually tested. Blocks were

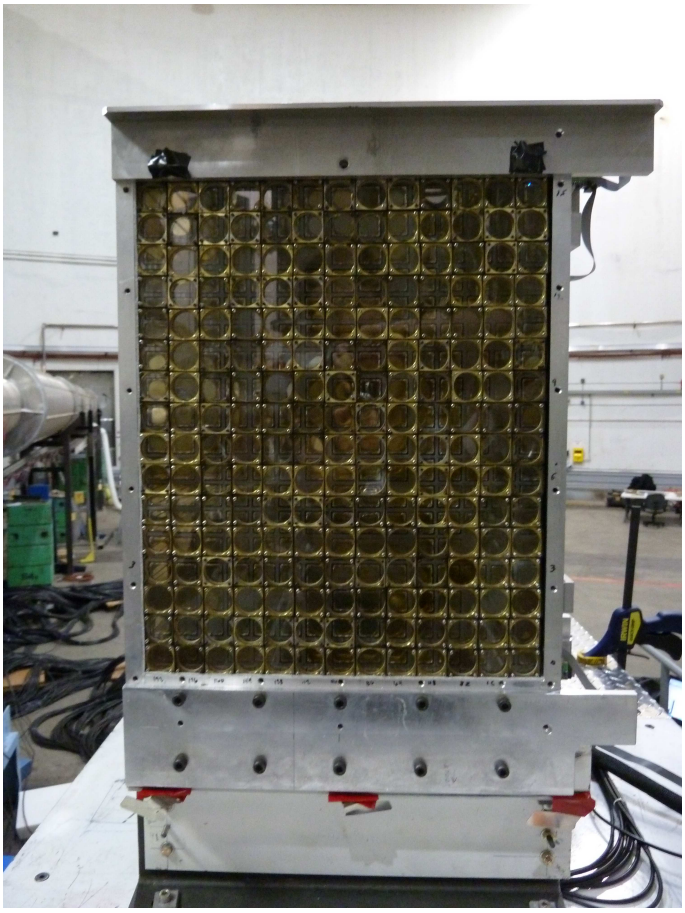

FIG. 2: Expanded DVCS calorimeter, as installed in Hall A in September 2010. View is from the target, with downstream beam pipe visible on the left.

irradiated using the 20 MeV electron beam of the Idaho Accelerator Center (IAC), and transparency loss measured as a function of time. This allowed us to put aside the less resistant blocks.

Fig. 3 shows the variation in gain between Oct 26 and Dec 14, 2010, during the execution of experiments E07-007/E08-025. Up to ∼25% transparency loss was observed for some blocks, but with typical variations of around ∼5%. Blocks closer to the beam line (higher block numbers) show a higher loss.

We performed 3 elastic ($ep \rightarrow ep$) calibrations of the DVCS calorimeter (p detected in HRS, e detected in the calorimeter) throughout the experiment. Tab. I shows the energy resolution achieved in each of one. As you can see, even though the transparency of blocks change with time, the resolution of the calorimeter remained roughly constant during the experiment. Note that the first 2 calibrations were performed at an electron energy of 3.2 GeV whereas the last one was at 3.9 GeV.

Preliminary online analyses of the 2010 DVCS data show that calorimeter was performing well:

- The $ep \rightarrow ep$ elastic calibration reproduces the expected energy resolution (Fig. 4 and Tab. I).

Date	E (GeV)	σ/E	$\sigma/\sqrt{E}$ (GeV$^{1/2}$)
Oct 26	3.2	3.1%	0.0555
Nov 17	3.2	3.1%	0.0555
Dec 14	3.9	2.8%	0.0553

TABLE I: Energy resolution for the different elastic calibrations of the DVCS calorimeter. Note that the 3rd one was made at a different electron energy (E).

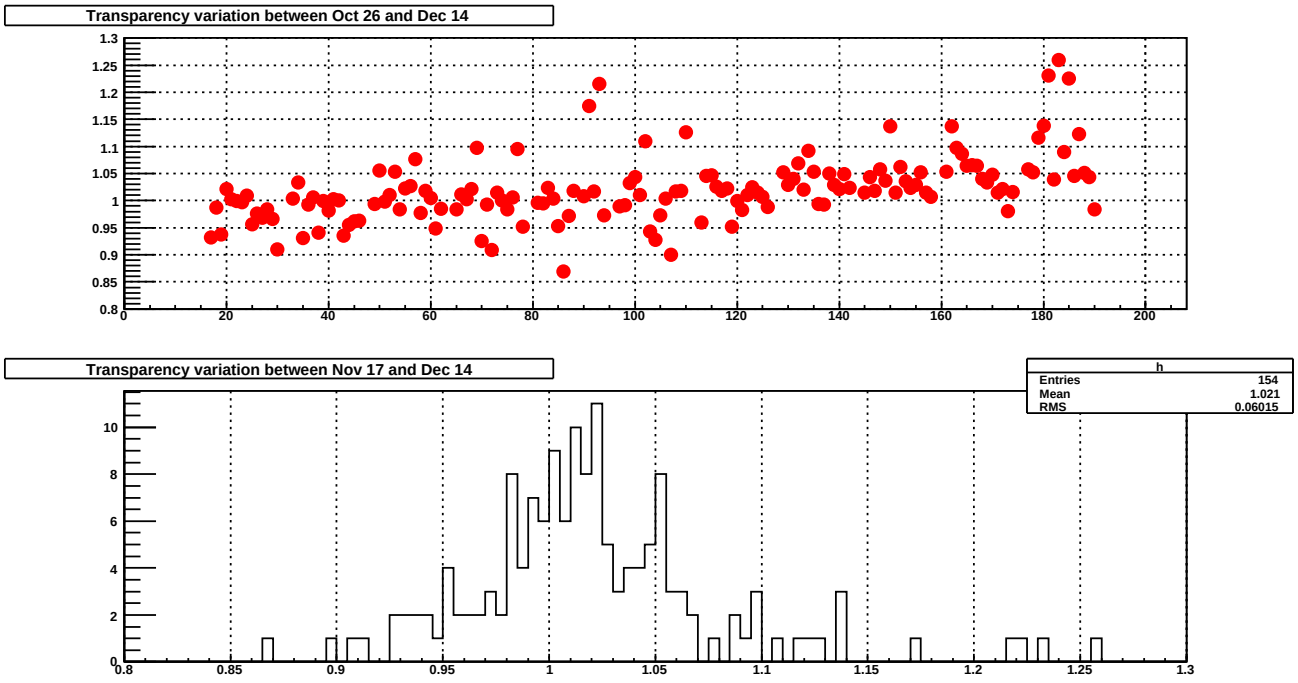

FIG. 3: Top: Ratio of calibration coefficients before and after 50 (calendar) days of data taking during E07-007/E08-025. The PbF_2 blocks are numbered from lower-right to upper left in the picture of Fig. 2. Each 16 consecutive channels is one column. Blocks at the edges of the calorimeter are omitted from the plot. The last 16 blocks in the plot are the next to last column adjacent to the beam line, and hence received the highest dose. Bottom: Histogram of ratios of calibration constants from top graph.

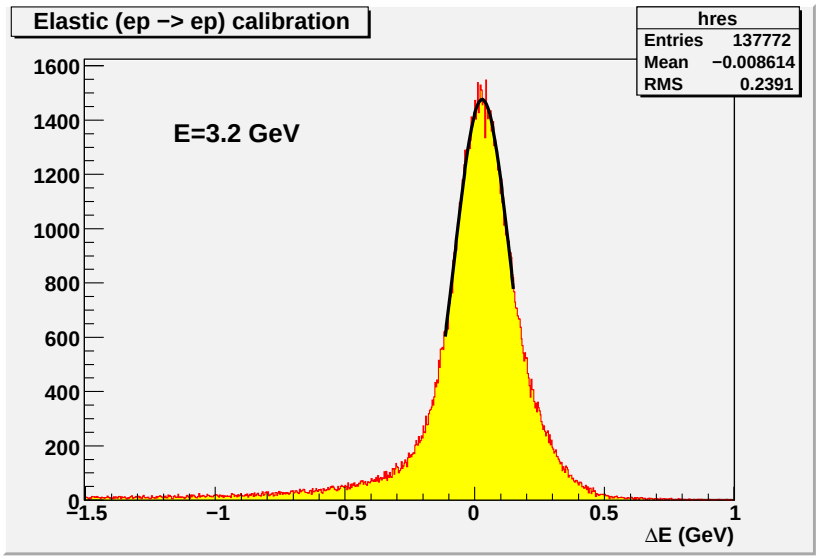

FIG. 4: DVCS calorimeter energy resolution: reconstructed energy minus electron energy (E) for $\langle E \rangle = 3.2$ GeV

.

- The $2-\gamma$ invariant mass reproduces the π^0 mass (Fig. 5, left).
- The $ep \to e\gamma X$ missing mass squared has the desired peak at the recoil nucleon mass squared (Fig. 5, right).

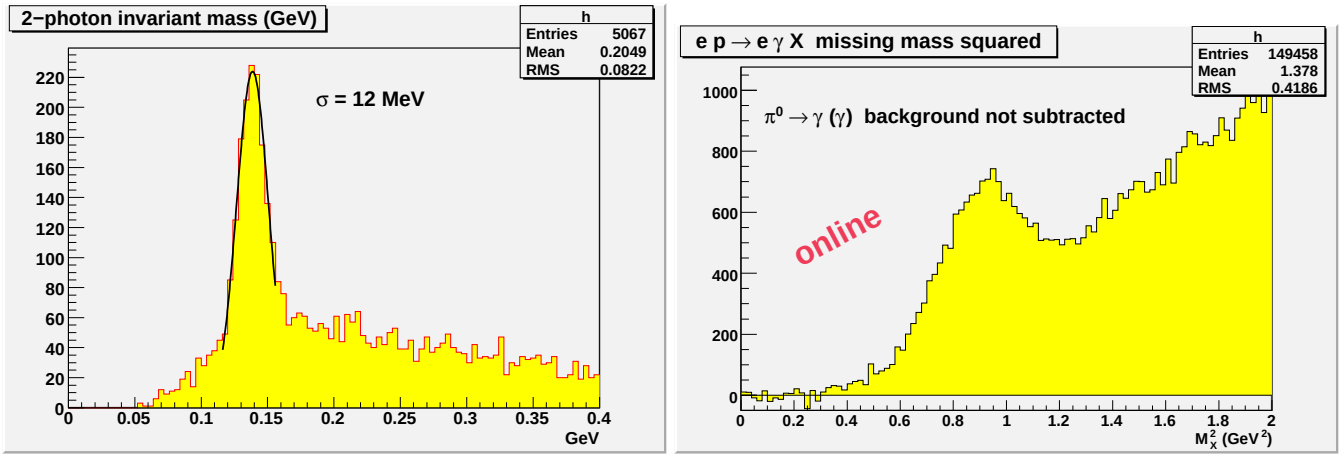

FIG. 5: Calorimeter performances: π^0 reconstructed mass (left) and $ep \to e\gamma X$ missing mass squared (right)

.

B. Other mechanical updates

All the mechanical upgrades concerning the expansion of the DVCS calorimeter have been accomplished. These include a new box and stand to hold the expanded version of the PbF_2 array (Fig. 6). The calorimeter stands on a moving cart which allows to change the distance to the target, between 1.0 and 5.5 m.

In the original proposal, we suggested replacing the downstream beam pipe by a conical one. During E07-007/E08-025 we added some W shielding at the intersection of the scattering chamber with the beam pipe and around the calorimeter-side of the downstream beam pipe. This way of shielding may be an alternate solution to the conical beam pipe. We plan to make a decision on this in the next few months, after further analysis of the 2010 data.

C. DVCS DAQ

Together with the expansion of the calorimeter, the DVCS DAQ was also upgraded. The DVCS DAQ has two distinct components:

- The Analog Ring Sampler (ARS) system that digitizes of the PMT signals and allows to remove pile-up offline. This improves both timing and energy resolution which would be otherwise degraded due to the pile-up from the high luminosity running.
- The DVCS coincidence trigger, which is a level-2 decision module that selects events with a cluster in the calorimeter above a programmable energy threshold.

The upgrade of the ARS system (Fig. 7, left) was two-fold. Firstly, the transfer protocol was upgraded from the VME protocol BLT32 to VME160SST. This resulted in a data transfer going from a maximum of 7 MBytes/s up to 94 Mbytes/s. Secondly, an event buffer was added in order to be able to take new data while transferring previous events. Both improvements reduced the acquisition deadtime. We thus managed to take roughly 10 times more data than the previous experiment with similar values of deadtime.

The upgrade of the DVCS trigger (Fig. 7, right) consisted in expanding the previous module in order to take into account the larger number of channels. Also, event buffering was implemented in the same way as for the ARS system. Several trigger options were available: overall energy threshold on the sum of all calorimeter blocks, or on local clusters formed by adjacent blocks. Finally, the resolution on the threshold was increased by using 12-bit (instead of 7-bit before) fast-ADCs to digitize signals.

III. SUMMARY

We propose to measure the absolute helicity-dependent and helicity-independent cross sections for the DVCS process as functions of Q^2 for several values of x_B, with $\sim 4\%$ systematic uncertainty and similar statistical uncertainty. This

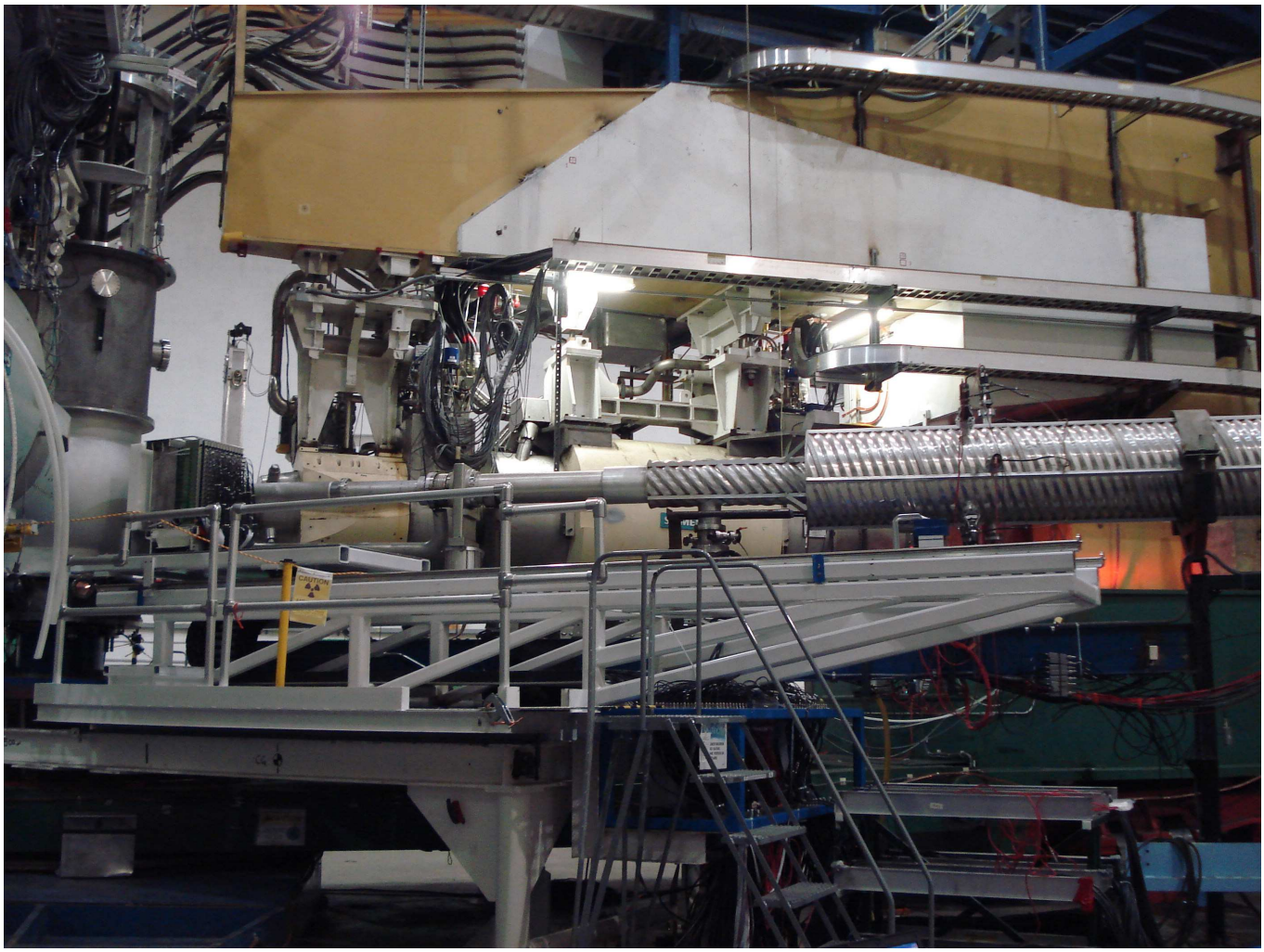

FIG. 6: DVCS scattering chamber and PbF_2 calorimeter on its cart and stand, as installed in Hall in September 2010. The calorimeter (without its light tight box) is visible immediately adjacent to the spherical scattering chamber. The HRS-Left is used to detect the scattered electron. For 11 GeV running, the calorimeter will be rolled back to various positions ranging from 1.5 to 3.0 m from the target vertex, as required for reconstruction of two photon clusters from exclusive π^0 events.

will provide stringent scaling tests of the real and the imaginary part of the DVCS amplitude, over a much larger kinematic domain than the one currently accessible.

The kinematics settings proposed in this experiment are shown in Fig. 8 and a summary of our beamtime request is described in Tab. II. For more details on the kinematics, please refer to Tab. V of the original proposal. In addition to the 88 days of beam, we request 12 days of overhead. These days will be used for calibrations of the calorimeter and/or curing radiation damage of blocks.

[1] C. Munoz Camacho et al. (Jefferson Lab Hall A), Phys. Rev. Lett. **97**, 262002 (2006), nucl-ex/0607029.
[2] M. Mazouz et al. (Jefferson Lab Hall A Collaboration), Phys. Rev. Lett. **99**, 242501 (2007), 0709.0450.
[3] E. Fuchey et al., Phys. Rev. **C83**, 025201 (2011), 1003.2938.
[4] F. X. Girod et al. (CLAS), Phys. Rev. Lett. **100**, 162002 (2008), 0711.4805.
[5] O. V. Teryaev (2005), hep-ph/0510031.
[6] I. V. Anikin and O. V. Teryaev, Fizika **B17**, 151 (2008), 0710.4211.
[7] I. V. Anikin and O. V. Teryaev, Phys. Rev. **D76**, 056007 (2007), 0704.2185.

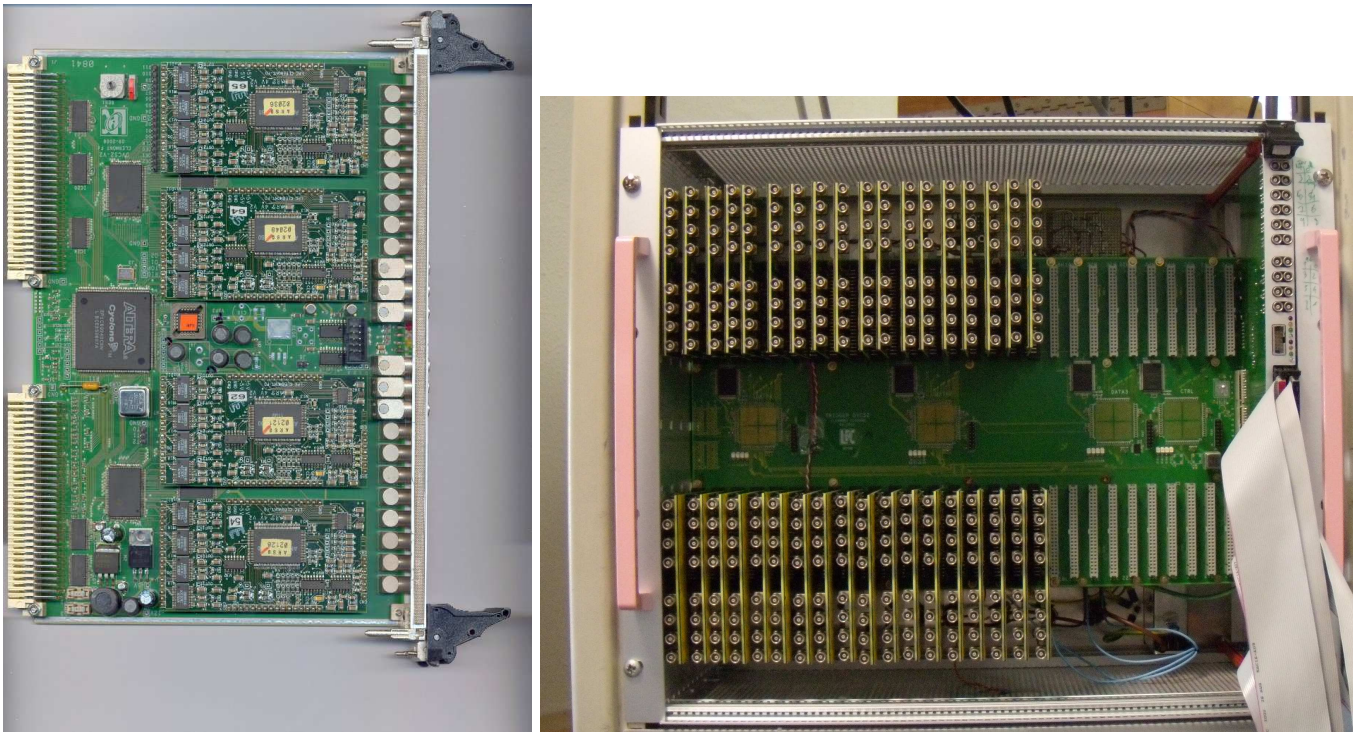

FIG. 7: Left: Upgraded ARS board for sampling the DVCS calorimeter PMT signals. Right: Upgraded calorimeter level-2 trigger module.

		Beam time (days)		
k	Q^2		$x_{\rm Bj}$	
(GeV)	(GeV^2)	0.36	0.50	0.60
6.6	3.0	3		
8.8	4.0	2		
11.0	4.55	1		
6.6	3.1		5	
8.8	4.8		4	
11.0	6.3		4	
11.0	7.2		7	
8.8	5.1			13
8.8	6.0			16
11.0	7.7			13
11.0	9.0			20
	Total	6	20	62

TABLE II: Summary of beam time request. In addition to the 88 days of beam, we request 12 days of overhead for calibration and/or bleaching of the DVCS calorimeter.

[8] M. Diehl and D. Y. Ivanov, Eur. Phys. J. **C52**, 919 (2007), 0707.0351.
[9] M. V. Polyakov and C. Weiss, Phys. Rev. **D60**, 114017 (1999), hep-ph/9902451.
[10] M. V. Polyakov and M. Vanderhaeghen (2008), 0803.1271.
[11] M. Guidal, Eur. Phys. J. **A37**, 319 (2008), 0807.2355.
[12] H. Moutarde, Phys. Rev. **D79**, 094021 (2009), 0904.1648.
[13] M. Guidal and H. Moutarde, Eur. Phys. J. **A42**, 71 (2009), 0905.1220.
[14] M. Guidal, Phys. Lett. **B689**, 156 (2010), 1003.0307.
[15] M. Guidal, Phys. Lett. **B693**, 17 (2010), 1005.4922.
[16] K. Kumericki and D. Mueller, Nucl. Phys. **B841**, 1 (2010), 0904.0458.
[17] G. R. Goldstein, J. O. G. Hernandez, and S. Liuti (2010), 1012.3776.

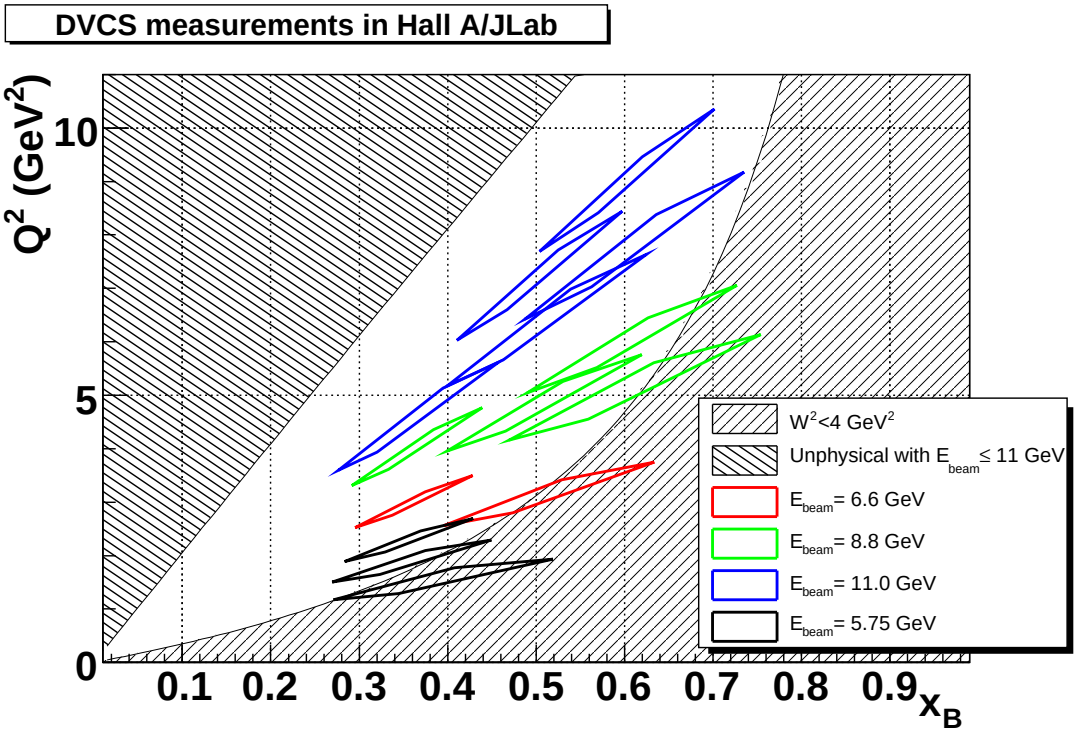

FIG. 8: Proposed DVCS kinematics for H$(e, e'\gamma)p$ measurements in Hall A with 3, 4, and 5 pass beams of CEBAF at 12 GeV. The diamond shapes trace the approximate acceptance of the HRS in each setting. The boundary of the unphysical region corresponds to the maximum possible Q^2 at a given x_B for 11 GeV. This corresponds to 180° electron scattering, equivalent to $\theta_q = 0°$. The points at $E_{Beam} = 5.75$ GeV were obtained in E00-110 and E07-007.

[18] K. Kumericki, D. Mueller, and A. Schafer (2011), 1106.2808.
[19] J. M. Laget, Phys. Lett. **B695**, 199 (2011), 1004.1949.
[20] M. M. Kaskulov and U. Mosel, J. Phys. Conf. Ser. **295**, 012112 (2011), 1101.6042.
[21] M. M. Kaskulov (2011), 1105.1993.
[22] S. V. Goloskokov and P. Kroll (2011), 1106.4897.